Computationally Efficient Power Integrity Simulation for System-on-Package Applications

Krishna Bharath[†], Ege Engin[‡] and
Madhavan Swaminathan[§]
School of Electrical and Computer Engineering
Georgia Institute of Technology
Atlanta, GA
{[†]kbharath, [‡]engin,
[§]madhavan.swaminathan}@ece.gatech.edu

Kazuhide Uriu[1] and Toru Yamada[2]
EMC Design Group
System Engineering Center
Matsushita Electric Industrial Co., Ltd.
{[1]uriu.kazuhide,
[2]yamada.-toru}@jp.panasonic.com

ABSTRACT

Power integrity simulation for system-on-package (SoP) based modules is a crucial bottleneck in the SoP design flow. In this paper, the multi-layer finite difference method (M-FDM) augmented with models for split planes has been proposed as a fast and accurate frequency domain engine. Results demonstrating the accuracy and scalability of the method have been presented. In particular, the algorithm was employed to the analysis of a realistic 6 layer package with $\sim$ 200k nodes.

Categories and Subject Descriptors

I.6 [**Computing Methodologies**]: Simulation and Modeling

General Terms

Algorithms, Design

Keywords

Signal/Power Integrity (SI/PI), System in Package (SiP), multi-layer finite difference method (M-FDM)

1. INTRODUCTION

Consumer demand for convergent systems is forcing the integration of multiple dissimilar components, such as high speed digital, RF and passives into a mixed-signal system-on-package (SoP) module.

An SoP containing four modules illustrating the various modes of coupling that can occur is shown in Figure 1. The digital module generates simultaneous switching noise (SSN) at multiples of the clock frequency, which can then couple to RF modules that are sensitive to SSN. For the case of a cell phone receiver, a -60dB insertion loss between the digital and RF modules can significantly degrade the performance of the front-end low-noise amplifier. Also, decreasing supply voltages coupled with increasing power requirements tends to place stringent requirements on the target impedance [11] of the digital part. Clearly, time-efficient and accurate signal and power integrity (SI/PI) simulation will be a critical component of the SoP design flow.

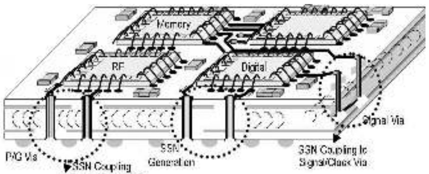

Figure 1: A System on Package Module.

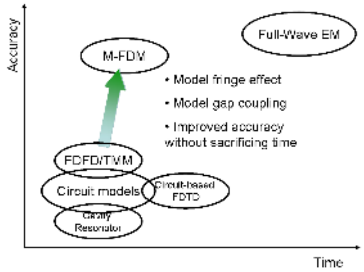

Figure 2: Accuracy vs. time comparisons for competing methods.

A system-level SI/PI co-simulation methodology was proposed in [10]. A key input to the proposed technique is the frequency response of the package. Figure 2 shows the performance of various available tools with respect to execution time and accuracy. 3D full-wave EM simulators are generally the most accurate tools available to obtain the frequency response. However, the inherent time and memory complexity involved relegates the use of these simulators to final verification, at which stage, the cost of fixing SI/PI problems can be prohibitive. On the other hand, circuit modeling techniques such as those based on the transmission line method (TLM) [2] have been proposed as alternate

DAC 2007, June 4–8, 2007, San Diego, California, USA.

methods. These methods are time efficient, but are not accurate when the power distribution network (PDN) contains holes. Recently, the multi-layer finite difference method (M-FDM) has been proposed in [4] to address this issue. In this paper, an overview of M-FDM will be presented. To ensure accurate results when the test structures contain split planes, the M-FDM formulation needs to be modified to model second order effects occurring due to fringe fields and coupling across slots. Fringe and gap models for single plane pair cases have been developed in [1] and will be extended in this paper. Also, for the first time, M-FDM will be applied to a six layer package structure to demonstrate its scalability.

The rest of the paper is organized as follows. In section 2, a brief overview of SSN, and the need to model apertures and split planes will be presented. The finite difference formulation for single plane pair geometries will be discussed in section 3, and its extension to multiple plane pairs (M-FDM) will be described in section 4. Addition of fringe and gap effects will be presented in section 5. Results illustrating the accuracy and the scalability of the method are shown in section 6, and conclusions are presented in section 7.

2. SSN COUPLING IN PACKAGE STRUCTURES

Figure 3 shows a three layer package PDN supplying power to a mixed-signal IC. Multiple power supplies are typically required in modern SoPs due to the various integrated components. Split planes are required to provide DC isolation to the different supply voltages. Also, holes are created in the solid power/ground planes in order to route signals or to provide via anti-pads. The switching activity of digital circuitry causes a time varying current to be drawn from its power supply terminals, Vdd1-Gnd1. Due to the associated inductance of the loop, SSN is generated. SSN can couple horizontally across a plane pair and across power islands. Also, SSN couples vertically through vias, and through apertures. This can be regarded as a coupling by means of a wrap-around current on the edges of the planes. Through these mechanisms, ground bounce can occur across the Vdd2-Gnd2 planes. Thus, it becomes critical to model split planes and apertures.

In [1], split planes have been modeled by employing lumped coupling elements. The values for these elements can be derived from closed form expressions based on the geometry of the problem. For narrow apertures, a transmission-line based model has been proposed to take into account interlayer coupling [7]. Electric and magnetic polarization currents have also been considered to compute coupling through electrically small cut-outs [9]. To the best of the authors' knowledge, M-FDM is the only efficient method available to analyze such structures with *arbitrarily large* holes in the planes.

3. M-FDM FOR SINGLE PLANE PAIR GEOMETRIES

The underlying elliptic partial differential equation for the modeling of planes is a Helmholtz equation

$$\left(\nabla_t^2 + k^2\right) u = -j\omega\mu d J_z \tag{1}$$

where ∇_t^2 is the transverse Laplace operator parallel to the planar structures, u is the voltage, d is the distance between

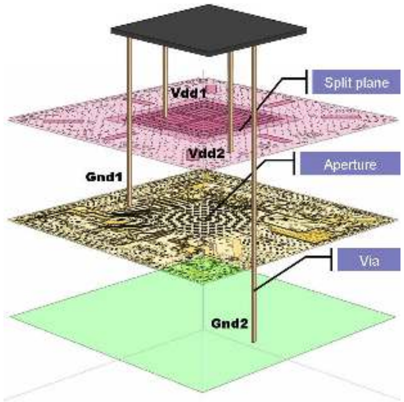

Figure 3: SSN coupling mechanisms in a realistic package.

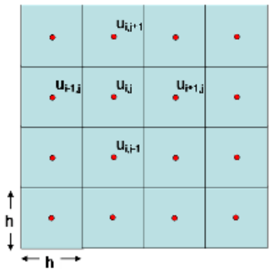

Figure 4: Discretization of the Laplace operator.

the planes, k is the wave number, and J_z is the current density injected normally to the planes [13]. The problem definition is completed by assigning homogenous Neumann boundary conditions, which correspond to assuming a magnetic wall, or an open circuit, on the periphery of the planes. One method to solve the Helmholtz equation is by applying the finite-difference scheme. The 2-dimensional Laplace operator can be approximated as

$$\nabla_t^2 u_{i,j} = \frac{u_{i,j+1} + u_{i+1,j} + u_{i,j-1} + u_{i-1,j} - 4u_{i,j}}{h^2} \tag{2}$$

, where h is the mesh length and $u_{i,j}$ is the voltage at node (i,j) for the cell-centered discretization shown in Figure 4.

This discretization results in a well-known bedspring unit cell model [4] for a plane-pair consisting of inductors (L) between neighboring nodes, and capacitors (C) from each node to ground. Figure 5 shows the equivalent circuit obtained by discretizing a plane-pair into unit cells. This equivalent circuit model can be solved using a standard circuit solver. However, direct solution of the M-FDM equation using a linear equation solver can improve the memory requirements and speed, since the resulting admittance matrix is a sparse banded matrix. Based on the plane model in Figure 5, a linear equation system can be obtained which can be written in matrix form as:

$$\overline{\overline{\mathbf{Y}}}\bar{U} = \bar{I} \tag{3}$$

where $\overline{U}$ and $\overline{I}$ are the cell voltage and current vectors. The matrix $\overline{\overline{\mathbf{Y}}}$ is the nodal admittance matrix. If the unit cells are numbered using natural ordering, $\overline{\overline{\mathbf{Y}}}$ has the following

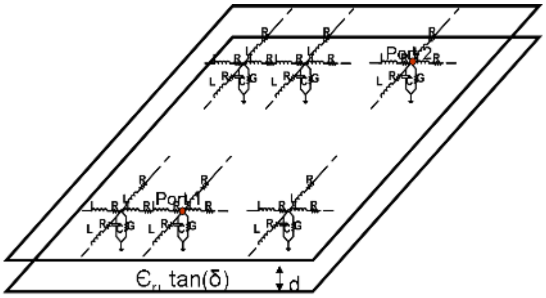

Figure 5: Electrical model for a plane-pair.

form:

$$\overline{\overline{\mathbf{Y}}} = \begin{pmatrix} A-B & B & & & B & & & \\ B & A-B & B & & & B & & \\ & B & \ddots & \ddots & & & \ddots & \\ B & & \ddots & A-2B & \ddots & & & \\ & \ddots & & \ddots & \ddots & \ddots & & \ddots \\ & & B & & & & B & A \end{pmatrix} \tag{4}$$

where, $A = j\omega C + \frac{1}{j\omega L}$ and $B = -\frac{1}{j\omega L}$. If the plane pair were to be discretized with M_1 cells horizontally and M_2 cells vertically, then the matrix $\overline{\overline{\mathbf{Y}}}$ is $N \times N$ where $N = M_1 M_2$. If unit cells are numbered along columns, the bandwidth of $\overline{\overline{\mathbf{Y}}}$ is M_2. Using a direct solver, the computational complexity for equation 3 is $O(N \times M_2^2)$. For typical geometries, $M_1 \approx M_2 \approx \sqrt{N}$, resulting in a complexity of $O(N^2)$. Also, if sparse storage is used, memory required is $O(N^{1.5})$. The method can be further enhanced by the use of nested dissection, which is an asymptotically optimal node ordering method. This can improve the flop count to $O(N^{1.5})$ and memory to $O(N \log_2 \sqrt{N})$ [5].

4. M-FDM EXTENSION TO INFINITE LAYERS

The unit cell model used in Figure 5 uses a common ground node. In a multilayered structure consisting of more than two planes, unit cells of different plane pairs can assign this ground potential to different planes. Therefore, such unit cells cannot be stacked on top of each other without any modification to model a multilayered plane. A straightforward stacking would short-circuit the elements between two ground connections, resulting in a completely erroneous model. To obtain a model for the combined unit cell representing all the planes in the structure, consider the inductor elements in a unit cell as shown in Figure 6(a). L1 is the per unit cell (p.u.c.) inductance between plane 1 and plane 2, whereas L2 is the inductance between plane 2 and 3. Hence, reference planes are different in both models in Figure 6(b) and L2 would be short-circuited if the same nodes on plane 2 were connected with each other. In order to avoid that, the p.u.c. inductances can be combined as shown in Figure 6(c) using a mutual inductance and assigning plane 3 as the reference plane. This model can be extended in a similar way to any number of planes. Physically, this model is based on the fact that there is a complete coupling of the magnetic field when the return current is on plane 3, as represented by the mutual inductance that is equal to L2.

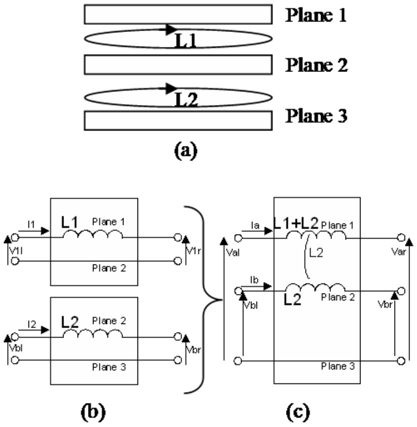

Figure 6: (a) Side view of a unit cell for a 3 plane structure showing the current loops associated with the p.u.c. inductances. (b) P.u.c. inductance of each plane pair. (c) Combining the p.u.c. inductances by changing the reference planes.

In terms of the admittance parameters, this model can be derived using the indefinite admittance matrix [3]. Following the formulation provided in [4], the total unit cell can be obtained as shown in Figure 7(b) for the example of three planes, where the bottom plane is chosen as the voltage reference plane. The equivalent circuit that would be obtained for a three layer geometry is shown in Figure 7(c). For solid multilayered rectangular planes, discretized with M_1 cells in the x-direction and with M_2 cells in the y-direction, the admittance matrix $\overline{\overline{\mathbf{Y}}}$ can be written as

$$\overline{\overline{\mathbf{Y}}} = \begin{pmatrix} \bar{\bar{A}} & \bar{\bar{B}} & & & \\ \bar{\bar{B}} & \bar{\bar{A}} - \bar{\bar{B}} & \bar{\bar{B}} & & \\ & \bar{\bar{B}} & \ddots & \ddots & \\ & & \ddots & \ddots & \bar{\bar{B}} \\ & & & \bar{\bar{B}} & \bar{\bar{A}} \end{pmatrix} \tag{5}$$

where $\bar{\bar{A}} =$

$$\begin{pmatrix} \bar{\bar{Y}}_{uc} + 2\bar{\bar{Z}}_{uc}^{-1} & -\bar{\bar{Z}}_{uc}^{-1} & & & & \\ -\bar{\bar{Z}}_{uc}^{-1} & \bar{\bar{Y}}_{uc} + 3\bar{\bar{Z}}_{uc}^{-1} & -\bar{\bar{Z}}_{uc}^{-1} & & & \\ & -\bar{\bar{Z}}_{uc}^{-1} & \bar{\bar{Y}}_{uc} + 3\bar{\bar{Z}}_{uc}^{-1} & \ddots & & \\ & & \ddots & \ddots & -\bar{\bar{Z}}_{uc}^{-1} & \\ & & & -\bar{\bar{Z}}_{uc}^{-1} & \bar{\bar{Y}}_{uc} + 3\bar{\bar{Z}}_{uc}^{-1} & -\bar{\bar{Z}}_{uc}^{-1} \\ & & & & -\bar{\bar{Z}}_{uc}^{-1} & \bar{\bar{Y}}_{uc} + 2\bar{\bar{Z}}_{uc}^{-1} \end{pmatrix} \tag{6}$$

and

$$\bar{\bar{B}} = \begin{pmatrix} -\bar{\bar{Z}}_{uc}^{-1} & & \\ & \ddots & \\ & & -\bar{\bar{Z}}_{uc}^{-1} \end{pmatrix} \tag{7}$$

Here, A and B are $kM_1 \times kM_1$ matrices for $(k+1)$ planes, assuming that the nodes are numbered starting from the top node in the lowest row, increasing in the vertical direction to the bottom node, then starting with the next cell in the x-direction until the last cell, and then starting with the next

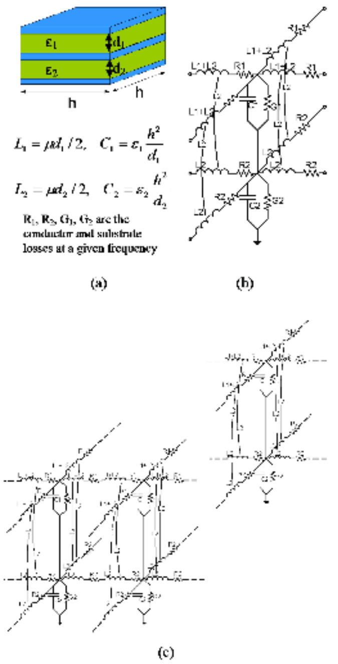

Figure 7: (a) Geometry and p.u.c. parameters. (b) Combined unit cell model for three planes. (c) Plane model consisting of multilayer unit cells.

row. Hence, $\overline{\overline{\mathbf{Y}}}$ is a $(kM_1M_2) \times (kM_1M_2)$ matrix. The unit cell matrices, $\bar{\bar{Y}}_{uc}$ and $\bar{\bar{Z}}_{uc}^{-1}$ are tri-diagonal and are given by

$$\bar{\bar{Y}}_{uc} = \begin{pmatrix} Y_1 & -Y_1 & & & \\ -Y_1 & Y_1+Y_2 & -Y_2 & & \\ & -Y_2 & \ddots & \ddots & \\ & & \ddots & \ddots & -Yk-2 \\ & & -Y_{k}-2 & Y_{k-2}+Y_{k-1} & -Y_{k-1} \\ & & & -Y_{k-1} & Y_{k-1}+Y_k \end{pmatrix} \quad (8)$$

and

$$\bar{\bar{Z}}_{uc}^{-1} = \begin{pmatrix} \frac{1}{Z_1} & -\frac{1}{Z_1} & & & \\ -\frac{1}{Z_1} & \frac{1}{Z_1}+\frac{1}{Z_2} & -\frac{1}{Z_2} & & \\ & -\frac{1}{Z_2} & \ddots & \ddots & \\ & & \ddots & \ddots & -\frac{1}{Z_{k-2}} \\ & & -\frac{1}{Z_{k-2}} & \frac{1}{Z_{k-2}}+\frac{1}{Z_{k-1}} & -\frac{1}{Z_{k-1}} \\ & & & -\frac{1}{Z_{k-1}} & \frac{1}{Z_{k-1}}+\frac{1}{Z_k} \end{pmatrix} \quad (9)$$

where Y_i and Z_i can be obtained similar to the unit cell parameters for a single plane pair structure as

$$Y_i = j\omega C_i + \omega C_i \tan\delta_i \quad (10)$$

$$Z_i = 2j\omega L_i + \frac{2}{\sigma t} + 2\sqrt{\frac{j\omega\mu}{\sigma}} \quad (11)$$

By an analysis similar to what was provided in the previous section, it can be shown that the computational complexity of M-FDM applied to $k+1$ layers is $O(N^2)$ where $N = (kM_1M_2)$. Typically in the presence of mutual inductor elements such as what has been shown in Figure 7, the unit cell inductance matrix $\bar{\bar{Z}}_{uc}^{-1}$ will be full-dense. However, the nature of the loop inductances considered lends to the tri-diagonal form shown in (9) and hence to the unique advantages of M-FDM.

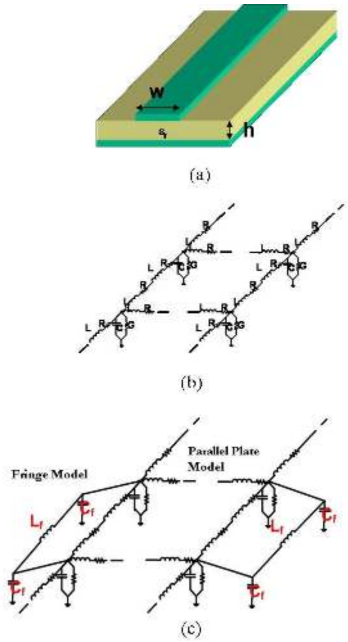

Figure 8: (a)Geometry (b)Representation with the FDFD model (c)Correction for fringe effect by addition of elements C_f and L_f.

5. INCLUSION OF SECONDARY EFFECTS

5.1 Fringe Effect Models

The M-FDM formulation discussed in the previous sections assumes that each unit cell sees plane-pairs of infinite extent along the lateral directions. However, fringing fields occur at edge discontinuities. This implies that both the per-unit-length (p.u.l) inductance and capacitance will be different from that obtained from parallel plate formulae. This problem has been considered in [6], which proposes building a library that maps various geometries to model elements, and interpolating between these values. However, this technique requires the development of a large database that accounts for variations in dielectric height and permittivity, trace width and metal height, and can suffer from interpolation errors. On the other hand, the technique proposed in [1] relies on well characterized closed form expressions which are easy to implement. The fringe fields are corrected by adding additional elements to edges. A microstrip line of width W, dielectric height h and metal thickness t is shown in Figure 8(a). The M-FDM model for this microstrip is shown in Figure 8(b). The fringe effect is modeled by the addition of L_f and C_f, as shown in Figure 8(c), and are given by [1]

$$C_f = \frac{C_{pul} - C_{pp}}{2} w \quad (12)$$

$$L_f = \frac{2\mu h w L_{pul}}{\mu h - W L_{pul}} \quad (13)$$

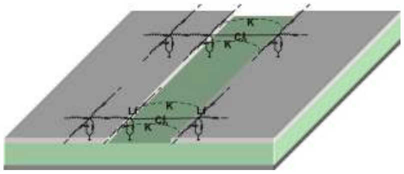

Figure 9: Gap model with addition of gap elements, Cm and K.

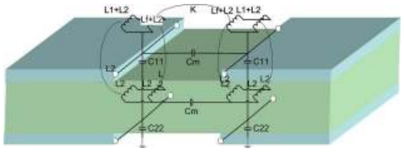

Figure 10: Equivalent circuit to model splits on both planes.

where, C_{pul} and L_{pul} are the p.u.l capacitance and inductance of a microstrip line of equivalent width, dielectric height h and permeability μ. C_{pp} is the p.u.l parallel plate capacitance and w is the unit cell width.

5.2 Gap Effect Models

Coupling occurs between physically separated metal patches when the distance of separation between them approaches the dielectric thickness. The coupling can be especially significant when the patches resonate. Figure 9 shows split planes of width W separated by a spacing s, with a dielectric height h. The gap is modeled by considering both the E-field and H- field coupling The E-field coupling is represented by a capacitor, C_m, connected between the nodes that lie across the gap. The H-field coupling is modeled by a mutual coupling factor, K, as shown in Figure 9. The values of C_m and K are obtained by applying coupled line theory as explained in [1]. However, this method has been proposed only for single plane pair geometries with split planes on one of the layers with the second layer being solid. It is possible to extend this to cases where split planes can occur on both layers. In Figure 10, an equivalent circuit is shown for this case. A third metal layer is introduced far away to act as a solid reference plane. The M-FDM formulation is now applied for this three layer geometry. The mutual elements C_m and K are introduced as shown in Figure 10. These parameters are obtained as before. A test structure containing split planes on both layers is shown in Figure 11. The method-of-moments based full-wave solver Sonnet was used for comparison. The insertion loss results have been plotted in Figure 12, and it can be seen that the results from M-FDM match well with Sonnet. This example illustrates how the gap models can be extended to multi-layer geometries.

The addition of the fringe models do not increase the complexity of the problem as they represent only a correction to existing circuit elements. However, the addition of the gap elements will increase the bandwidth of the admittance matrix, as the width of a split plane may be discretized by more than one unit cell. However, it is known that coupling between patches becomes less significant as the ratio of the gap spacing s to the dielectric height h becomes large, for which the gap model may not be applied. This allows the computational complexity of the proposed approach to be maintained at $O(N^2)$.

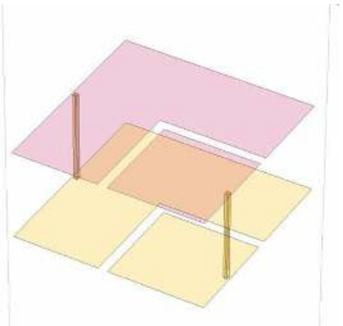

Figure 11: Test case with split planes on both layers. Size: 10 mm*10mm, $\epsilon = 4.4$, dielectric height = 300 μm.

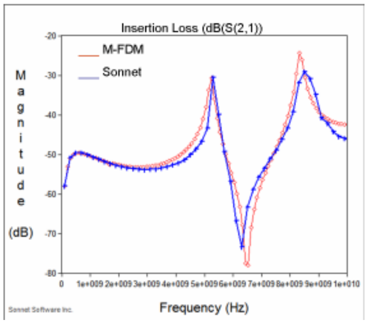

Figure 12: Insertion loss results for test case of Figure 11.

6. RESULTS

The methodology described in prior sections has been implemented in a CAD tool. Simulations were performed to compare the methodology against full-wave simulations and measurements, and to demonstrate the scalability of the method. All simulations were performed on an Intel Xeon workstation with a 3.2 GHz processor and 3.5 GB of RAM. Full-wave simulations were performed with the method-of-moments based solver, Sonnet.

The layout for two of the power distribution layers from a realistic package has been shown in Figure 13. The layers were discretized using a unit cell size of 0.185 mm, resulting in 38,800 nodes per layer. Table 1 shows the scalability of the simulation tool as the number of layers, and hence, the number of nodes is increased. These results do not follow the strict $O(N^2)$ characteristics predicted, as a generic sparse solver was used. For the six layer simulation with 194,000 nodes, the CAD tool required 12 minutes per frequency point. In comparison, even the simulation of the 2 layer example was intractable with Sonnet due to insufficient memory available.

To demonstrate the accuracy of the method, we consider a single plane pair example with the geometry of the top layer shown in Figure 14. This is an example containing several

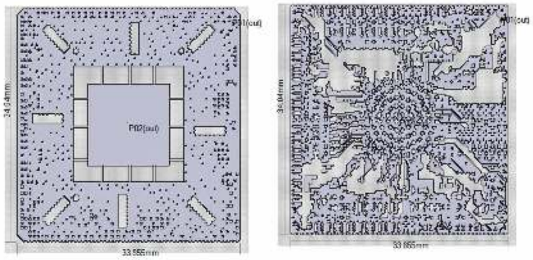

Figure 13: Layouts for two package layers. Dimension is 34mm × 34mm.

Table 1: Simulation results for realistic package.

Layers	Nodes	Time/Freq Point (s)
2	38, 800	1.5
3	77, 600	5.2
4	116, 400	72.5
5	155, 200	276.2
6	194, 000	725.27

holes as well as split planes, and hence can be used to establish the validity of the M-FDM formulation augmented with fringe and gap models. However, even for this example, Sonnet required 50 GB of memory. To create an example which could be simulated with Sonnet, the two outlined metal patches were considered in isolation, and the mesh was made coarse. This reduces the memory required by the full-wave solver to 200 MB. The insertion loss results have been plotted in Figure 15, and are virtually indistinguishable. The runtime for M-FDM was 2.1 s/freq. point vs. 124 s/freq. pt. for Sonnet, representing a speedup of 60X.

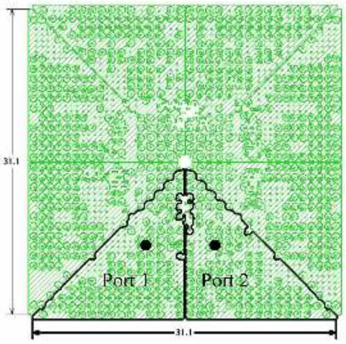

Figure 14: Geometry of split planes, dielectric thickness = 100 μm, $\epsilon_r = 4.4$. All dimensions are in mm.

7. CONCLUSION

The emergence of package level integration as a dominant contender for convergent systems has led to the need for efficient CAD tools for power integrity analysis. In this paper, a fast and accurate method based on finite differences was proposed. Results demonstrating the accuracy and scalability of the method have been shown.

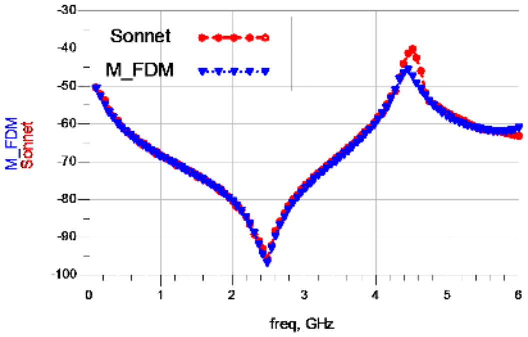

Figure 15: Insertion loss (dB) results for highlighted structure of Figure 14.

8. REFERENCES

[1] K. Bharath, E. Engin, M. Swaminathan, K. Uriu, and T. Yamada. Efficient modeling of package power delivery networks with fringing fields and gap coupling in mixed signal systems. In *Proc. of 15th IEEE EPEP*, pages 59–62, Oct. 2006.

[2] C. Christopoulos. *The Transmission-Line Modeling Method: TLM.* Wiley-IEEE Press, 1995.

[3] J. A. Dobrowolski. *Introduction to Computer Methods for Microwave Circuit Analysis and Design.* Artech House, 1991.

[4] E. Engin, K. Bharath, M. Swaminathan, and et. al. Finite-difference modeling of noise coupling between power/ground planes in multilayered packages and boards. In *Proc. of 56th ECTC*, pages 1262 – 1267, June 2006.

[5] A. George. Nested dissection of a regular finite element mesh. *SIAM Journal on Numerical Analysis*, 10(2):345–363, April 1973.

[6] C.-C. Huang and C. Luk. Accurate analysis of multi-layered signal and power distributions using the fringe rlgc models. In *Proc. of 13th IEEE EPEP*, pages 103–106, Oct. 2004.

[7] R. Ito and R. Jackson. Parallel plate slot coupler modeling using two dimensional frequency domain transmission line matrix method. In *Proc. of 13th IEEE EPEP*, pages 41–44, Oct. 2004.

[8] J. Kim and M. Swaminathan. Modeling of multilayered power distribution planes using transmission matrix method. *IEEE Trans. Adv. Packag*, 25(2):189–199, May 2002.

[9] J. Lee, M. Rotaru, M. Iyer, H. Kim, and J. Kim. Analysis and suppression of ssn noise coupling between power/ground plane cavities through cutouts in multilayer packages and pcbs. *IEEE Trans. Adv. Packag.*, 28(2):298–309, May 2005.

[10] R. Mandrekar, K. Bharath, K. Srinivasan, E. Engin, and M.Swaminathan. System level signal and power integrity analysis methodology for system-in-package applications. In *Proc. of 43rd DAC*, pages 1009 – 1012, July 2006.

[11] P. Muthana, M. Swaminathan, E. Engin, P. M. Raj, and R. Tummala. Mid frequency decoupling using embedded decoupling capacitors. In *Proc. of 14th EPEP*, pages 271 – 274, Oct. 2005.

[12] N. Na, J. Choi, S. Chun, M. Swaminathan, and J. Srinivasan. Modeling and transient simulation of planes in electromagnetic packages. *IEEE Trans. Comp., Packag., Manufact. Technol.*, 21:157–163, May 1998.

[13] E. T. Itoh. *Numerical Techniques for Microwave and Millimeter-Wave Passive Structures.* John Wiley, 1989.